

WIND-TUNNEL TEST OF A
PHOTOVOLTAIC CONCENTRATOR ARRAY

by

J. A. Peterka,* J. J. Lou,**
and J. E. Cermak***

for

Martin Marietta Aerospace
Denver Division
Post Office Box 179
Denver, Colorado 80201

Fluid Mechanics and Wind Engineering Program
Fluid Dynamics and Diffusion Laboratory
Department of Civil Engineering
Colorado State University
Fort Collins, Colorado 80523

June 1979

*Associate Professor
**Research Associate
***Director, Fluid Dynamics
and Diffusion Laboratory



U18401 0075235

CER78-79JAP-JJL-JEC62

TABLE OF CONTENTS

<u>Chapter</u>	<u>Page</u>
LIST OF TABLES	iii
LIST OF FIGURES	iv
LIST OF SYMBOLS	v
1. INTRODUCTION	1
2. EXPERIMENTAL CONFIGURATION	3
2.1 Wind Tunnel	3
2.2 The Models	3
3. INSTRUMENTATION AND DATA ACQUISITION	5
3.1 Measurements of Forces and Moments	5
3.2 Measurements of Flow Characteristics	6
4. TEST PROCEDURES	8
5. TEST RESULTS	9
5.1 Forces and Moments	9
5.2 A Numerical Example	13
6. CONCLUSIONS	14
REFERENCES	15
TABLES	16
FIGURES	24

LIST OF TABLES

<u>Table</u>		<u>Page</u>
1	Test Matrix for Operational Force and Torque Measurements [Part (a) of Phase I]	17
2	Edge of Array Field Test Matrix [Part (a) of Phase II]	18
3	Center of Array Field Test Matrix [Part (b) of Phase II]	18
4	Force and Moment Coefficients for a Single Array [Part (a) of Phase I, see Table 1]	19
5	Force and Moment Coefficients [Part (b) of Phase I] . . .	20
6	Force and Moment Coefficients [Part (c) of Phase I] . . .	21
7	Force and Moment Coefficients [Part (a) of Phase II] . . .	22
8	Force and Moment Coefficients [Part (b) of Phase II] . . .	23

LIST OF FIGURES

<u>Figure</u>		<u>Page</u>
1	INDUSTRIAL AERODYNAMICS WIND TUNNEL.	25
2	PHOTOGRAPHS OF SINGLE PHOTOVOLTAIC CONCENTRATOR MODEL AND TYPICAL CLUSTER CONFIGURATION IN THE WIND TUNNEL	26
3a	MODEL CONFIGURATION.	27
3b	MODEL CONFIGURATION.	28
4	DEFINITION OF COORDINATE SYSTEM.	29
5	ARRAY CLUSTER CONFIGURATION.	30
6	FLOW CHARACTERISTICS IN THE INDUSTRIAL WIND TUNNEL DURING TESTS.	31
7	MOMENT TRANSFER FROM M_y TO M_{p_y}	32
8	DETERMINATION OF CENTER OF PRESSURE.	32
9	ARRAY IN STOWED POSITION AT 10° ANGLE (PART C OF PHASE I).	33
10	EFFECTS OF ADJACENT ARRAY (a) UNBALANCED SHIELDING, (b) CHANNELING	34

LIST OF SYMBOLS

A_{ref}	=	constant reference area (379.8 in. ² model, 379.8 ft ² full-scale)-approximate array face area
AZ	=	azimuth angle of the array
$C_{F_x}, C_{F_y}, C_{F_z}$	=	nondimensional forces coefficients in x, y and z
$C_{M_x}, C_{M_y}, C_{M_z}$	=	nondimensional moment coefficients about the x, y and z axes at the base of the model
C_{MP_x}, C_{MP_y}	=	nondimensional moment coefficients about the pivot center of the model
D_V, D_H	=	location of center of pressure on array face due to component of force perpendicular to face
EL	=	elevation angle
F_x, F_y, F_z	=	measured force along x, y and z axes, respectively
L_{ref}	=	reference length (9.1 in. model, 9.1 ft full-scale)-approximate array chord
M_x, M_y, M_z	=	measured moment about x, y and z axes, respectively
M_{p_x}, M_{p_y}	=	moment about x_p and y_p axes
U_{30}	=	reference free stream velocity at 30 in. model
X, Y, Z	=	Cartesian coordinate system
ν	=	kinematic viscosity of air
ρ	=	density of air
$\frac{UL}{\nu}$	=	Reynolds number
$\frac{1}{2} \rho U_{30}^2$	= q =	reference dynamic pressure

1. INTRODUCTION

The purpose of this investigation was to determine wind forces and moments acting on a photovoltaic concentrator array, both as an isolated structure and as part of a multiple-array field. The flow around a single array or around a cluster of arrays is complex and thus makes the use of exact theoretical analysis virtually impossible. However, properly designed studies on structural models in wind tunnels can yield quantitative data for the analysis of wind loading.

To model the aerodynamic loading on a structure, careful attention must be given to similarity requirements for the flow (simulated wind) and the model structure to insure that results may be scaled from model to prototype. In general, the requirements are: (1) undistorted scaling of boundary geometry (geometric similarity), (2) kinematic similarity of approach flow (distribution of mean wind speed and turbulence characteristics), and (3) Reynolds number equality. Details concerning these requirements and their wind-tunnel implementation can be found in references 1, 2 and 3.

These criteria are satisfied by testing the scale model of the prototype structure and its surroundings (in this study, a flat, open area) in a wind tunnel capable of modeling atmospheric boundary-layer flows. However, Reynolds number ($\frac{UL}{\nu}$) similarity cannot always be met in existing wind tunnels. If the same fluid is used, wind velocity in the wind tunnel would have to be as large as the model scale factor times the prototype wind velocity--a condition leading to undesirable compressibility effects. Above a certain critical Reynolds number (2×10^4) there is no significant change in the values of the aerodynamic coefficients if the model is characterized by sharp edges. Typical

values of Reynolds number encountered are 10^7 - 10^8 for the full-scale and 10^5 - 10^6 for the wind-tunnel model. Thus, Reynolds number invariance between model and prototype is achieved at velocities well below those used in the model study.

The similarity of turbulence structure between wind tunnel and full-scale cannot be demonstrated for model scales as large as the 1:12 scale used for this study. The boundary-layer flow typically shows correct scaling for 1:200 to 1:400 models. The modeling for the 1:12 case suffers in two respects: lower turbulence intensity and smaller integral scale of turbulence in the wind-tunnel flow than would exist for a complete similarity. Because the integral scale of turbulence in the wind tunnel is much larger than the typical dimensions of the model, the lack of an integral scale as large as complete similarity would dictate should not provide significant change in results (4). Change in turbulence intensity has been shown to cause changes in aerodynamic coefficients (4). Based on limited available data, the influence of turbulence intensity for this study should not be large for the single array, and should be insignificant for the cases where adjacent arrays are included since turbulence structure is then dominated by the wake structure of the upwind arrays.

2. EXPERIMENTAL CONFIGURATION

2.1 Wind Tunnel

The wind-tunnel study was performed in the Industrial Aerodynamic Wind Tunnel located in the Fluid Dynamics and Diffusion Laboratory at Colorado State University. The tunnel is a closed circuit facility driven by a 75 hp variable-pitch propeller. The test section is nominally 6 ft square, 60 ft long and is fed through a 4 to 1 ratio contracting section about 10 ft long. The roof is adjustable in height to maintain a zero pressure gradient along the test section. The mean velocity can be adjusted continuously from 1 to 65 fps. A schematic drawing of this tunnel is shown in Fig. 1.

2.2 The Models

An existing 1/12 scale model of the Martin Marietta low-profile photovoltaic array was supplied by the sponsor. A photograph of the model is shown in Fig. 2. This model could be pivoted about both elevation and azimuth axes and was modified to adapt to a six-component force balance transducer as shown in Figs. 3 and 4. The model is 41.8 in. by 9.1 in. with slits to give approximately 18 percent porosity.

The adjacent array models, also made available by the sponsor, were used to influence the wind streams acting on the instrumented model. These models, made from plywood, modeled the basic shape of the collector, but not the porosity. They were mounted to the floor of the wind tunnel and were adjustable to give desired elevation and azimuth angles. The cluster configuration of the photovoltaic concentrator array is shown in Fig. 5 while Fig. 2 shows portions of the cluster array in a test configuration.

The instrumented model was mounted on a 63 in. diameter turntable. The turntable indicated azimuthal angle of the array to about 0.2 degrees. The wind-tunnel ceiling was then adjusted, after mounting of the model(s), to obtain a zero pressure gradient along the test section.

3. INSTRUMENTATION AND DATA ACQUISITION

3.1 Measurements of Forces and Moments

Mean force and moment measurements on the instrumented model were made using an Inca six-component strain-gage balance. Three forces and three moments were measured on the model. The balance was aligned with its axes in an x, y and z coordinate system fixed to the model according to Figs. 3 and 4.

Each strain-gage bridge of the balance was monitored by a Honeywell Accudata 118 Gage Control/Amplifier unit which provided excitation to the bridge and amplified the bridge output. These instruments are characterized by a stable excitation voltage and amplifier gain. Each channel signal was further processed through a low-pass filter and then fed by means of analog lines specially designed to minimize distortion to a Preston Model GMAD-4 analog-to-digital converter. The data was then analyzed by a Hewlett-Packard System 1000 minicomputer under program control.

All six transducers were recorded simultaneously for three minutes at a 40 sample per second rate.

Calibration of the balance was performed in a test rig in which known forces and moments could be applied to the balance. A calibration matrix was then obtained for reducing the mean output of the strain gages. The load and strain relationship is linear in the range of loads applied in this study. The force balance and electronic system are supported by their manufactured specifications to be accurate to within 0.1 percent of full-scale. This would indicate a possible error of 2.5 percent in the force and moment measurements.

Note that the existing force and moment measurements are average values and do not contain gust loading. Thus, the peak forces and moments for gust loading must be obtained by using a quasi-static loading assumption and an estimated gust velocity. This study did not attempt to determine aeroelastic response.

3.2 Measurements of Flow Characteristics

Velocity and turbulence intensity profiles for the approach flow under test conditions were made at the location of the model (turntable) in the tunnel with the model removed.

The measurements were made with a Thermosystems Model 1050 constant-temperature anemometer with a 0.001 in. diameter platinum film sensing element 0.02 in. long. The sensing probe was attached to a vertical traverse to measure velocities and turbulent intensities at different heights. Output was read from a Hewlett-Packard integrating digital voltmeter (Model 2401C) for mean voltage and a DISA rms meter (Model 55D35) for rms voltage.

The wind-tunnel floor was textured to provide a velocity profile which varied with a power-law relationship in height (0.14 power-law exponent). The reference velocity was obtained by using a standard pitot-static tube in an undisturbed area upstream from the model at a height 48 in. above the tunnel floor. However, force and moment coefficient were nondimensionalized by the dynamic pressure $\frac{1}{2} \rho U_{30}^2$, where U_{30} is the velocity at the scaled height of 30 ft (30 in. model).

Tests were made at only one wind speed in the tunnel. This wind speed was sufficiently high to ensure Reynolds number similarity between the model (10^5) and the prototype (10^7).

The measured characteristics of the flow field (Fig. 6) are similar to the average characteristics of the atmospheric boundary layer as discussed by Cermak (1) for small scale models (1:200 to 1:400).

4. TEST PROCEDURES

The photovoltaic array test was comprised of two phases: individual array and array field tests.

Phase I--Individual Array Tests

- (a) Operational Torques and Forces: 56 tests at selected combinations of 8 wind azimuths and 11 elevation angles were conducted as shown in Table 1.
- (b) Maximum Moments: Tests were made at 2° azimuth increments where maximum moments were found in Ia above in order to obtain the true maximum values. Cases with a solid overlay covering the face of the model to eliminate porosity were also studied.
- (c) Maximum Bending Moment: One test with the elevation (y_p) axis parallel to the wind approach direction with the array in the stowed position (face down) but with the y_p axis inclined 10° to horizontal to simulate a 10° angle of attack was conducted.

Phase II--Array Field Tests

- (a) Edge of Array Field: This configuration was simulated by incorporating dummy arrays A and C of Fig. 5 adjacent to the instrumented array. Two additional tests were made to study the effect of increasing the distances between two arrays. Refer to Table 2 for tests run.
- (b) Center of Array Field: This configuration was simulated by incorporating dummy arrays A, B, C and D of Fig. 5 adjacent to the instrumented array. Tests conducted are shown in Table 3.

5. TEST RESULTS

5.1 Forces and Moments

The forces and moments measured on the photovoltaic concentrator array are expressed in terms of nondimensional coefficients C_F , C_M and C_{MP} . They are defined as follows:

force coefficient along the x-axis (drag coefficient)

$$C_{F_x} = \frac{F_x}{\left(\frac{1}{2} \rho U_{30}^2\right) A_{\text{ref}}}$$

force coefficient along the y-axis (lateral force coefficient)

$$C_{F_y} = \frac{F_y}{\left(\frac{1}{2} \rho U_{30}^2\right) A_{\text{ref}}}$$

force coefficient along the z-axis (lift force coefficient)

$$C_{F_z} = \frac{F_z}{\left(\frac{1}{2} \rho U_{30}^2\right) A_{\text{ref}}}$$

moment coefficient about the x-axis at the base of the model (see Fig. 4)

$$C_{M_x} = \frac{M_x}{\left(\frac{1}{2} \rho U_{30}^2\right) (A_{\text{ref}}) (L_{\text{ref}})}$$

moment coefficient about the y-axis at the base of the model (see Fig. 4)

$$C_{M_y} = \frac{M_y}{\left(\frac{1}{2} \rho U_{30}^2\right) (A_{\text{ref}}) (L_{\text{ref}})}$$

moment coefficient about the z-axis (azimuth torque)

$$C_{M_z} = \frac{M_z}{\left(\frac{1}{2} \rho U_{30}^2\right) (A_{\text{ref}}) (L_{\text{ref}})}$$

moment coefficient about the x_p -axis at the pivot center
(see Fig. 4)

$$C_{MP_x} = \frac{M_{P_x}}{\left(\frac{1}{2} \rho U_{30}^2\right) (A_{ref}) (L_{ref})}$$

moment coefficient about the y_p -axis at the pivot center (elevation
torque, see Fig. 4)

$$C_{MP_y} = \frac{M_{P_y}}{\left(\frac{1}{2} \rho U_{30}^2\right) (A_{ref}) (L_{ref})}$$

where

U_{30} = reference velocity at 30 ft (30 in. model),

ρ = density of air,

A_{ref} = constant reference area (379.8 in.² model, 379.8 ft² full-scale), approximate array face area

L_{ref} = reference length (9.1 in. model, 9.1 ft full-scale), approximate array chord

F_x, F_y, F_z = measured forces (drag, lateral and lift) along x , y and z axes,

M_x, M_y, M_z = moments about x , y and z axes at floor level, and

M_{P_x}, M_{P_y} = moments about pivot axes x_p, y_p .

The force and moment coefficients for a single photovoltaic array are given in Table 4. All but one data set were obtained with the front face of the array facing generally upwind. As expected, the maximum drag coefficient occurs with the array oriented normal to the wind (EL = 0°, AZ = 0°). Maximum bending moment (M_y) about the ground level also occurred for the same position. Maximum azimuth torque, C_{M_z} , was observed at EL = 0° and AZ = -45° and had the value 0.12.

The following equations were used to transfer moments to the pivot point. The moment M_y can be expressed in terms of the resultant force R (see Fig. 7):

$$M_y = F_x L - F_z D ,$$

This moment (M_y) can be transformed into the moment based on the pivot center of the photovoltaic concentrator (M_{p_y}).

$$M_{p_y} = -F_x (H-L) - F_z D$$

Subtracting these two equations,

$$M_{p_y} - M_y = -F_x H$$

$$M_{p_y} = M_y - F_x H$$

By similar arguments,

$$M_{p_x} = M_x - F_y H$$

D_V and D_H represent distances from the pivot center (origin of x_p, y_p axes) to the location of the force acting perpendicular to the collector face. They are obtained from the following calculations (see Fig. 8):

$$F_{\perp} = \vec{F}_x \cdot \vec{n} + \vec{F}_z \cdot \vec{n}$$

where \vec{n} is the unit normal vector to the photovoltaic collector surface.

$$D_V = \frac{(M_p / F_{\perp})}{L_{ref}}$$

$$M_{//} = \vec{M}_{P_x} \cdot \vec{t} + \vec{M}_z \cdot \vec{t}$$

where \vec{t} is the unit tangential vector.

$$D_H = \frac{(M_{//}/F_{\perp})}{L_{ref}}$$

Maximum elevation torque $|C_{MP_y}| = 0.05$ occurs at $EL = -60^\circ$ and $AZ = 0^\circ$.

Table 5 shows results of the tests made at 2° azimuth increments where maximum moments were found in the data of Table 4 (Phase I, Part b). Coefficients obtained with the array covered with a solid sheet are somewhat larger than those of the uncovered array.

Results for the array in the stowed position with elevation axis at 10° to the horizontal (Phase I, Part c), see Fig. 9, are shown in Table 6. The absolute magnitude of the C_{MP_x} torque has increased with $|C_{MP_x}| = 0.05$ ($EL = -90^\circ$ and $AZ = +90^\circ$), compared with the worst case $|C_{MP_x}| = 0.048$ where $EL = -30^\circ$ and $AZ = -45^\circ$ (Table 4). However, the maximum C_{MP_x} of Table 6 was obtained with a solid cover while data of Table 4 was with 18 percent porosity.

Tables 7 and 8 show the effect of adjacent arrays on the instrumented model. There is a significant reduction in drag force; thus adjacent arrays provide a significant shielding effect. In the edge-of-array-field case, the unbalanced shielding caused an increase in azimuth moment [see Table 7 ($EL = 0^\circ$, $AZ = 0^\circ$) and Fig. 10a]. The value $|C_{M_z}|$ was 0.28 as compared with single array 0.12. Tests were made with the distance S between two arrays increased from 36 in. to 54 in. The shielding effect in drag was reduced and the azimuth torque was also reduced by increasing S .

In the center-of-array-field case, azimuth moment at $EL = 0^\circ$ and $AZ = 30^\circ$ is rather high ($|C_{M_z}| = 0.26$). It appears that the flow was directed in the direction of the "channel" formed by the two upstream arrays, and thus produced "one-sided" loading on model surface (see Fig. 10b).

5.2 A Numerical Example

To illustrate the use of tabulated force and moment coefficients, the maximum drag force and bending moment acting on a single photovoltaic array is calculated for a wind speed of 100 ft/sec at 30 ft elevation. The reference area A_{ref} is 379.8 sq ft and reference length $L_{ref} = 9.1$ ft for the full-scale array. According to Table 4 the maximum drag coefficient is $C_{F_x} = 0.80$ and the maximum bending moment coefficient is $C_{M_x} = 0.45$ at $AZ = 0^\circ$ and $EL = 0^\circ$.

Assume the following conditions at the site:

Temperature = $80^\circ F$

Barometric pressure = 26.20 in. Hg

Then, air density, $\rho = 0.0020$ slugs/ft³

These will give a dynamic pressure

$$q = \frac{1}{2} \rho U^2 = (0.5)(0.0020)(100)^2 = 10 \text{ lbs/ft}^2.$$

The total drag would thus be

$$F_x = C_{F_x} q A_{ref} = (0.80)(10)(379.8) = 3040. \text{ lbs.}$$

The maximum bending moment is

$$M_x = C_{M_x} q A_{ref} L_{ref} = (0.45)(10)(379.8)(9.1) = 15550. \text{ ft-lbs.}$$

6. CONCLUSIONS

Mean wind forces and moments acting on a 1:12 scale model photovoltaic array with 18 percent porosity were measured in a wind tunnel for various configurations. Aerodynamic force and moment coefficients were obtained in the Reynolds number independence regime. The airflow characteristics produced in the wind tunnel were similar to those expected to occur in a flat, open area.

Drag coefficients C_{F_x} ranged in value up to 0.8 while overturning moments about ground level ranged up to 0.45 for conditions tested. Lateral force coefficients C_{F_y} ranged up to 0.16; vertical force coefficients C_{F_z} ranged up to 0.45. C_{M_y} values ranged up to 0.45. Moment coefficients about the x and z axes were much smaller than C_{M_y} ranging up to values of about 0.12. Elimination of porosity raised the maximum C_{F_x} and C_{M_y} values to 0.87 and 0.49 respectively and increased the maximum C_{M_z} from 0.12 to 0.40. Addition of surrounding array panels tended to substantially reduce both force and moment values. C_{F_x} and C_{M_y} values approached single array values for the edge array configuration [Part (a) of Phase II] when the upstream array was moved substantially upstream. C_{M_z} was increased for some geometries.

REFERENCES

1. Cermak, J. E., "Aerodynamics of Buildings," Annual Review of Fluid Mechanics, Vol. 8, 1976.
2. Cermak, J. E., "Laboratory Simulation of the Atmospheric Boundary Layer," AIAA Jl., Vol. 9, September, 1971.
3. Cermak, J. E., "Application of Fluid Mechanics to Wind Engineering," A Freeman Scholar Lecture, ASME Jl. of Fluids Engineering, Vol. 97, No. 1, March, 1975.
4. Bearman, P. W., "Turbulence Effects on Bluff Body Mean Flow," Proceedings Third U.S. National Conference on Wind Engineering Research, University of Florida, March, 1978.

TABLES

Table 1. Test Matrix for Operational Force and Torque Measurements
[Part (a) of Phase I]

EL \ AZ	0°	-15°	-30°	-45°	-60°	-75°	-90°	-135°
-90°	X	X	X	X	X	X	X	
-75°	X		X		X		X	
-60°	X	X	X	X	X	X	X	
-55°	X				X			
-45°	X		X		X		X	
-30°	X	X	X	X	X	X	X	
-15°	X		X		X		X	
0°	X	X	X	X	X	X	X	
+30°	X		X	X	X		X	X
+60°	X	X	X		X		X	
+75°	X		X		X			

X - Test Conducted

Table 2. Edge of Array Field Test Matrix
[Part (a) of Phase II]

EL \ AZ	0°	-30°	-45°	-60°	-90°
-60°	X	X	X		X
-30°	X	X	X		X
0°	X	X	X	X	X
+90°	X	X		X	

Table 3. Center of Array Field Test Matrix
[Part (b) of Phase II]

EL \ AZ	0°	-30°	-45°	-60°	-90°
-60°	X	X			X
-30°	X	X			X
0°	X	X		X	X
+90°	X	X			

Table 4. Force and Moment Coefficients for a Single Array
[Part (a) of Phase I, see Table 1]

ELEVATION ANGLE (degrees)	AZIMUTH ANGLE (degrees)	C_{F_x}	C_{F_y}	C_{F_z}	C_{M_x}	C_{M_y}	C_{M_z}	C_{MP_x}	C_{MP_y}	D_V	D_H
0	0	0.80	0.01	-0.12	-0.01	0.45	-0.02	-0.004	0.006	.007	-.028
0	-15	0.78	0.05	-0.13	-0.03	0.44	0.04	-0.004	0.003	.003	.054
0	-30	0.71	0.09	-0.16	-0.05	0.39	0.10	-0.001	-0.01	-.014	.146
0	-45	0.54	0.12	-0.14	-0.06	0.30	0.12	0.010	-0.007	-.012	.217
0	-60	0.37	0.13	-0.10	-0.07	0.20	0.09	0.005	-0.008	-.023	.243
0	-75	0.17	0.09	-0.05	-0.04	0.09	0.04	0.005	-0.003	-.017	.254
0	-90	0.01	0.04	-0.01	-0.02	0.00	0.0	-0.002	0.007	--	--
-15	0	0.78	0.01	-0.34	-0.02	0.42	-0.03	-0.012	-0.018	-.021	-.037
-15	-30	0.65	0.09	-0.32	-0.02	0.35	0.09	0.035	-0.015	-.021	.031
-15	-60	0.32	0.12	-0.18	-0.04	0.17	0.07	0.023	-0.01	-.026	.202
-15	-90	-0.03	0.04	-0.01	-0.03	0.01	-0.01	-0.007	--	--	--
-30	0	0.64	0.01	-0.40	-0.01	0.32	-0.02	-0.008	-0.036	-.047	-.027
-30	-15	0.61	0.05	-0.43	-0.01	0.32	0.02	0.012	-0.027	-.036	.003
-30	-30	0.54	0.10	-0.38	-0.01	0.28	0.06	0.047	-0.027	-.040	.114
-30	-45	0.43	0.13	-0.32	-0.02	0.21	0.07	0.048	-0.031	-.057	.153
-30	-60	0.27	0.12	-0.22	-0.03	0.14	0.04	0.035	-0.015	-.044	.153
-30	-75	0.13	0.08	-0.11	-0.03	0.06	0.02	0.009	-0.01	-.062	.109
-30	-90	0.00	0.05	-0.00	-0.04	-0.01	-0.01	-0.01	--	--	--
-45	0	0.49	0.00	-0.45	-0.02	0.24	-0.02	-0.020	-.035	-.053	-.033
-45	-30	0.42	0.10	-0.42	-0.01	0.21	0.03	0.046	-0.028	-.046	.091
-45	-60	0.18	0.12	-0.23	-0.04	0.10	0.02	0.029	0.004	.013	.109
-45	-90	-0.01	0.05	-0.00	-0.04	0.00	-0.01	--	--	--	--
-55	0	0.35	0.00	-0.43	-0.02	0.17	-0.01	-.013	-.030	-.053	-.030
-55	-60	0.16	0.11	-0.22	-0.04	0.06	0.00	.026	-.025	-.092	.083
-60	0	0.31	0.00	-0.39	-0.02	0.12	-0.01	-.013	-.050	-.101	-.037
-60	-15	0.29	0.06	-0.39	-0.02	0.13	0.00	.016	-.034	-.072	.026
-60	-30	0.27	0.10	-0.38	-0.03	0.12	0.00	.024	-.035	-.075	.042
-60	-45	0.21	0.12	-0.31	-0.05	0.08	-0.00	.024	-.031	-.085	.053
-60	-60	0.14	0.11	-0.22	-0.05	0.05	-0.01	.012	-.030	-.115	.030
-60	-75	0.04	0.07	-0.09	-0.04	0.02	-0.01	-.006	-.006	-.059	-.086
-60	-90	0.00	0.05	-0.01	-0.04	-0.01	-0.01	-.015	--	--	--
-75	0	0.19	0.00	-0.26	-0.01	0.07	-0.01	--	-.038	-.128	--
-75	-30	0.16	0.08	-0.26	-0.06	0.06	-0.02	-.011	-.028	-.095	-.052
-75	-60	0.05	0.08	-0.14	-0.05	0.03	-0.01	-.005	-.004	-.024	-.049
-75	-90	0.01	0.05	0.00	-0.04	0.00	0.00	--	--	--	--
-90	0	0.09	-0.01	0.01	-0.00	0.07	-0.01	--	.014	--	--
-90	-15	0.09	0.02	0.01	-0.02	0.06	-0.01	-.009	.011	--	--
-90	-30	0.08	0.05	0.00	-0.03	0.05	-0.01	-.009	.004	--	--
-90	-45	0.06	0.06	0.00	-0.04	0.03	-0.01	-.008	-.001	--	--
-90	-60	0.04	0.06	-0.01	-0.05	0.02	-0.01	-.010	-.001	--	--
-90	-75	0.02	0.06	-0.02	-0.05	0.01	0.00	-.014	-.001	--	--
-90	-90	0.02	0.05	-0.01	-0.04	-0.01	0.00	-.013	-.027	--	--
+30	0	0.68	0.00	0.25	0.01	0.40	-0.02	--	.025	.034	--
+30	-30	0.59	0.09	0.15	-0.09	0.34	0.08	-.042	.009	.015	.155
+30	-45	0.47	0.12	0.11	-0.11	0.27	0.09	-.044	.003	.007	.205
+30	-60	0.31	0.12	0.04	-0.11	0.18	0.07	-.039	.006	.020	.275
+30	-90	0.01	0.04	-0.01	-0.04	0.01	0.01	-.014	.003	--	--
+30	-135*	-0.37	0.16	--	-0.05	-0.21	-0.07	-.015	.033	--	.205
+60	0	0.35	0.00	0.29	0.01	0.24	-0.01	--	.045	.107	--
+60	-15	0.34	0.06	0.21	-0.05	0.22	-0.00	-.019	.032	.088	.043
+60	-30	0.31	0.10	0.21	-0.10	0.21	0.01	-.043	.033	.098	.128
+60	-60	0.19	0.12	0.09	-0.10	0.09	0.01	-.036	-.015	-.085	.211
+60	-90	-0.01	0.04	0.00	-0.04	0.01	0.01	--	--	--	--
+75	0	0.30	0.00	0.25	0.01	0.21	-0.01	.015	.041	0.131	-.053
+75	-30	0.25	0.10	0.21	-0.10	0.18	0.00	-.044	.037	.136	.162
+75	-60	0.13	0.11	0.10	-0.10	0.09	0.01	-.046	.013	0.103	0.353

*Front of array facing downwind

Table 5. Force and Moment Coefficients [Part (b) of Phase I]

ELEVATION ANGLE	AZIMUTH ANGLE	C_{F_x}	C_{F_y}	C_{F_z}	C_{M_x}	C_{M_y}	C_{M_z}	C_{MP_x}	C_{MP_y}	D_V	D_H
(maximum C_{M_z})											
0	-51	0.47	0.12	-0.10	-0.07	0.26	0.11	+.002	-.001	-.001	.234
0	-47	0.52	0.12	-0.11	-0.06	0.29	0.12	.003	-.007	-.012	.225
0	-45	0.55	0.12	-0.16	-0.06	0.30	0.12	.010	-.003	-.005	.222
0	-44	0.55	0.11	-0.12	-0.05	0.30	0.12	.008	-.003	-.005	.215
0	-43	0.55	0.11	-0.13	-0.06	0.32	0.12	-.002	.008	.014	.219
0	-41	0.57	0.11	-0.12	-0.06	0.32	0.12	.006	.000	.000	.206
(maximum C_{M_y})											
0	-4	0.78	0.02	-0.13	-0.02	0.45	-0.01	-.005	.012	.014	-.014
0	-2	0.80	0.01	-0.15	-0.01	0.45	-0.01	-.002	.005	.005	-.018
0	0	0.80	0.01	-0.12	-0.01	0.45	-0.03	-.004	.006	.007	-.032
0	+2	0.78	0.00	-0.13	-0.00	0.45	-0.04	-.001	.007	.009	-.046
0	+4	0.80	-0.00	-0.10	-0.00	0.46	-0.04	--	.008	.010	--
0	+6	0.80	-0.01	-0.12	0.00	0.45	-0.05	--	.005	.005	--
(maximum C_{M_y} and C_{M_z} with zero porosity cover)											
0	-45	0.85	0.00	-0.15	0.03	0.48	0.40	--	.007	.008	--
0	-30	0.84	0.01	-0.19	0.01	0.46	0.20	-.007	-.007	-.008	.242
0	-2	0.86	0.02	-0.08	-0.01	0.48	0.02	0.0	.001	-.000	.020
0	0	0.87	0.01	-0.20	-0.01	0.49	-0.01	-.003	.004	.004	-.017
0	+2	0.85	0.01	-0.16	-0.01	0.48	-0.05	-.006	.001	.001	-.060
0	+4	0.87	0.01	-0.15	-0.01	0.48	-0.09	-.009	-.004	-.004	-.100
(maximum C_{MP_y})											
-60	-2	0.32	0.01	-0.38	-0.01	0.13	-0.01	-.009	-0.047	-.096	-.029
-60	0	0.32	0.00	-0.38	-0.02	0.13	-0.01	-.014	-.052	-.106	-.038
-60	+2	0.32	-0.00	-0.38	-0.02	0.13	-0.01	--	-.047	-.096	--
(maximum C_{MP_y} with zero porosity cover)											
-60	-2	0.34	0.01	-0.55	-0.01	0.11	-0.01	-.003	-.082	-.128	-.009
-60	0	0.35	-0.00	-0.57	-0.03	0.11	-0.01	--	-.087	-.130	--
-60	+2	0.34	-0.00	-0.55	-0.04	0.11	-.002	--	-.078	-.119	--

Table 6. Force and Moment Coefficients [Part (c) of Phase I]

ELEVATION ANGLE	AZIMUTH ANGLE	C_{F_x}	C_{F_y}	C_{F_z}	C_{M_x}	C_{M_y}	C_{M_z}	C_{MP_x}	C_{MP_y}	C_{MP_z}	D_V	D_H
-90	+90	-0.01	-0.10	-0.16	0.07	-0.01	0.00	-0.0168	-0.001	0.00	0.002	0.096
-90	+90*	-0.01	-0.08	-0.14	0.01	0.00	0.00	-0.056	--	0.00	--	0.368
-90	+45*	0.08	-0.11	-0.27	0.06	0.07	0.00	-0.012	-0.0078	0.00	0.026	0.042
-90	-90	+0.01	+0.13	0.05	-0.13	0.00	0.00	-0.005	--	0.00	--	-0.73

*Data taken with solid cover

Table 7. Force and Moment Coefficients [Part (a) of Phase II]

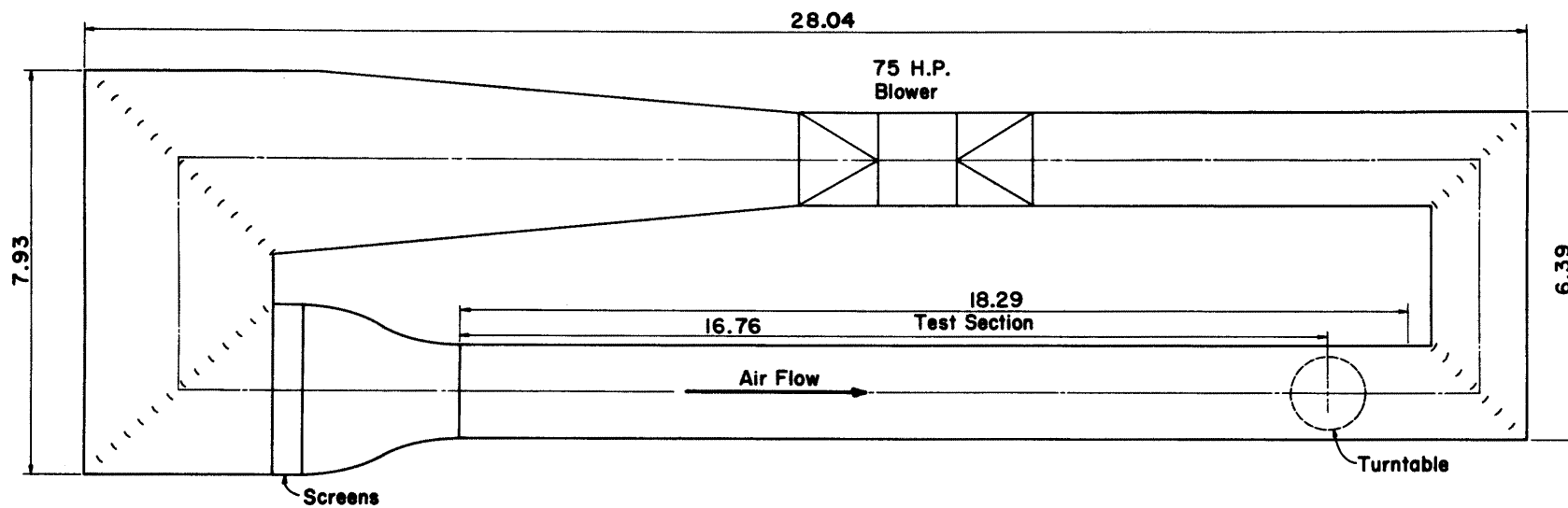
ELEVATION ANGLE	AZIMUTH ANGLE	C_{F_x}	C_{F_y}	C_{F_z}	C_{M_x}	C_{M_y}	C_{M_z}	C_{MP_x}	C_{MP_y}	D_V	D_H
+90	-90	0.03	0.05	-0.01	-0.05	-0.01	0.00	-.018	--	--	--
+90	-60	0.03	0.06	0.00	-0.04	0.03	-0.01	-.011	.011	--	--
+90	-30	0.05	0.07	-0.01	-0.04	0.03	-0.01	-.008	.001	.0751	--
0	-90	0.02	0.03	0.00	-0.02	-0.00	0.00	-.004	--	--	.0183
0	-60	0.28	0.09	-0.10	-0.05	0.16	0.04	-.005	.005	.0163	.1456
0	-45	0.36	0.06	-0.10	-0.05	0.20	-0.15	-.020	-.000	-.0093	-.418
0	-30	0.37	0.02	-0.04	-0.03	0.21	-0.29	-.020	.008	.0228	-.783
0	0	0.47	-0.05	-0.06	0.01	0.27	-0.28	-.022	.005	.0107	-.586
0*	-45	0.48	0.08	-0.10	-0.04	0.27	0.07	-.008	.001	.563	.152
0*	0	0.70	-0.03	-0.08	0.01	0.40	-0.10	-.010	.005	.567	-.145
-30	-90	0.02	0.05	-0.00	-0.03	-0.01	-0.01	-.007	--	--	-.747
-30	-60	0.25	0.10	-0.16	-0.03	0.11	0.02	.024	-.027	-.0907	.096
-30	-45	0.31	0.08	-0.21	-0.12	0.14	-0.15	-.077	-.028	-.0753	-.444
-30	0	0.48	-0.05	-0.33	-0.10	0.24	-0.22	--	-.027	-.0458	--
-60	-90	0.01	0.05	-0.00	-0.04	0.03	-0.01	-.014	.026	--	--
-60	-60	0.12	0.09	-0.19	-0.04	0.05	-0.01	.006	-.016	-.0718	-.0083
-60	-45	0.17	0.09	-0.24	-0.13	0.06	-0.08	-.082	-.035	-.1195	-.376
-60	0	0.27	0.00	-0.36	-0.07	0.11	-0.08	--	-.042	-.0932	--

*Distance S between two arrays = 54 inches (see Fig. 5)

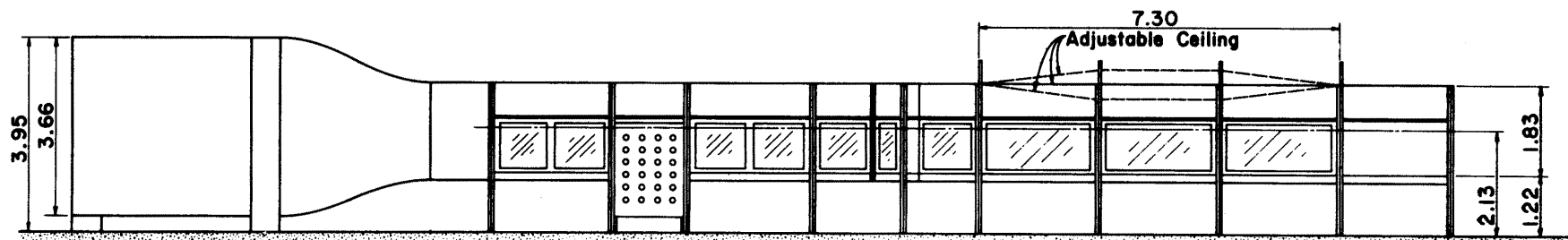
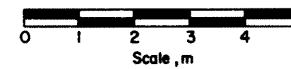
Table 8. Force and Moment Coefficients [Part (b) of Phase II]

ELEVATION ANGLE	AZIMUTH ANGLE	C_{F_x}	C_{F_y}	C_{F_z}	C_{M_x}	C_{M_y}	C_{M_z}	C_{MP_x}	C_{MP_y}	D_V	D_H
+90	-90	0.01	0.05	-0.00	-0.05	-0.01	0.00	-.017	--	--	--
+90	-60	0.03	0.06	0.01	-0.04	0.02	-0.01	-.012	.005	--	--
0	-90	-0.00	0.04	0.00	-0.02	0.00	0.00	--	--	--	--
0	-60	0.27	0.09	-0.08	-0.05	0.14	0.04	0.003	-.010	-.0342	.169
0	-30	0.23	0.03	-0.00	-0.04	0.13	-0.26	-.003	-.002	-.0067	-1.116
0	0	0.01	-0.00	0.14	0.00	-0.01	0.00	--	--	--	--
-30	-90	-0.01	0.05	0.00	-0.04	0.00	-0.01	--	--	--	--
-30	-60	0.23	0.10	-0.16	-0.03	0.11	0.02	.024	-.014	-.0493	.116
-30	0	0.08	-0.00	-0.06	0.00	0.05	0.01	--	.004	.0398	--
-60	-90	-0.01	0.04	0.00	-0.04	-0.00	-0.01	--	--	--	--
-60	-60	0.13	0.09	-0.21	-0.05	0.05	-0.01	-.003	-.024	-.0966	-.031
-60	0	0.16	0.00	-0.23	-0.00	0.07	-0.00	-.003	-0.020	-.0072	-.0034

FIGURES



PLAN



All Dimensions in m

ELEVATION

FIGURE 1. INDUSTRIAL AERODYNAMICS WIND TUNNEL

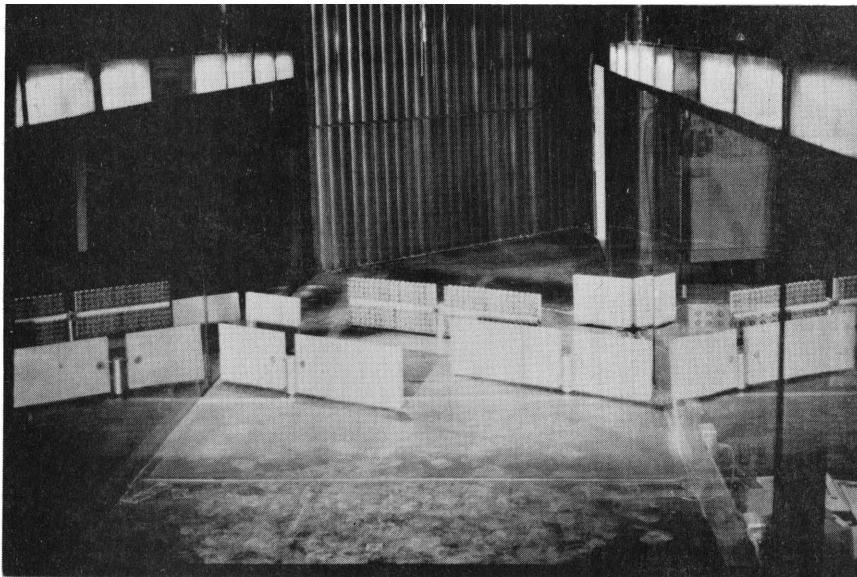
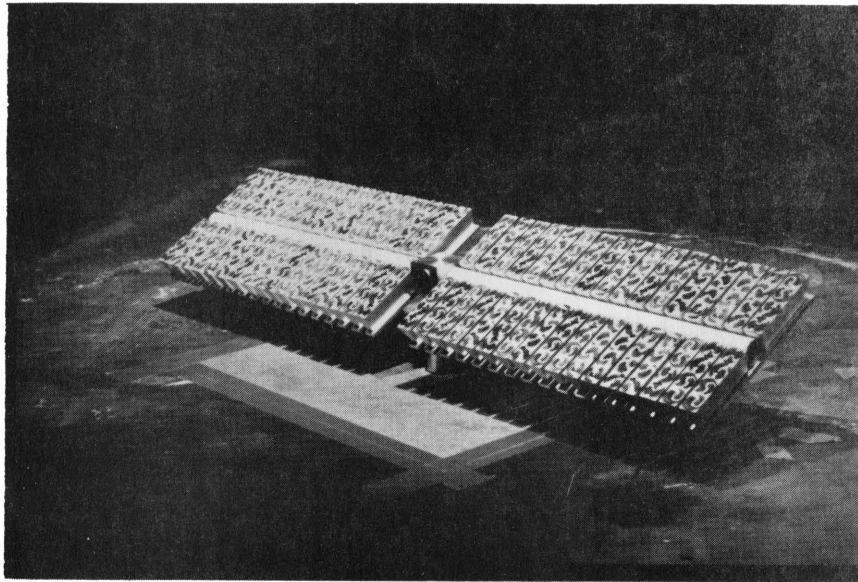
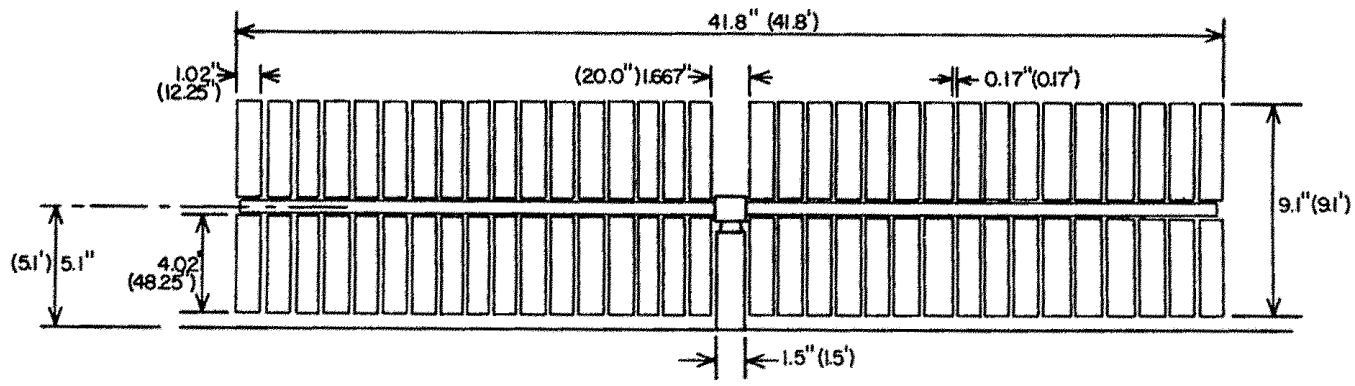
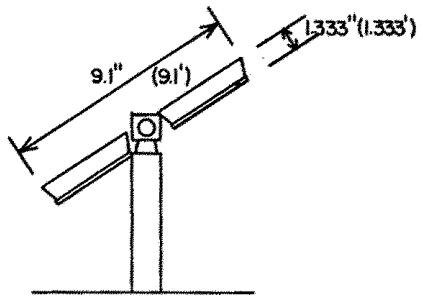


FIGURE 2. PHOTOGRAPHS OF SINGLE PHOTOVOLTAIC CONCENTRATOR MODEL AND TYPICAL CLUSTER CONFIGURATION IN THE WIND TUNNEL



ARRAY FRONT VIEW
ELEVATION ANGLE = 0°



SIDE VIEW
ELEVATION ANGLE = -57°

DIMENSIONS GIVEN ARE :
MODEL (FULL SCALE)

FIGURE 3a. MODEL CONFIGURATION

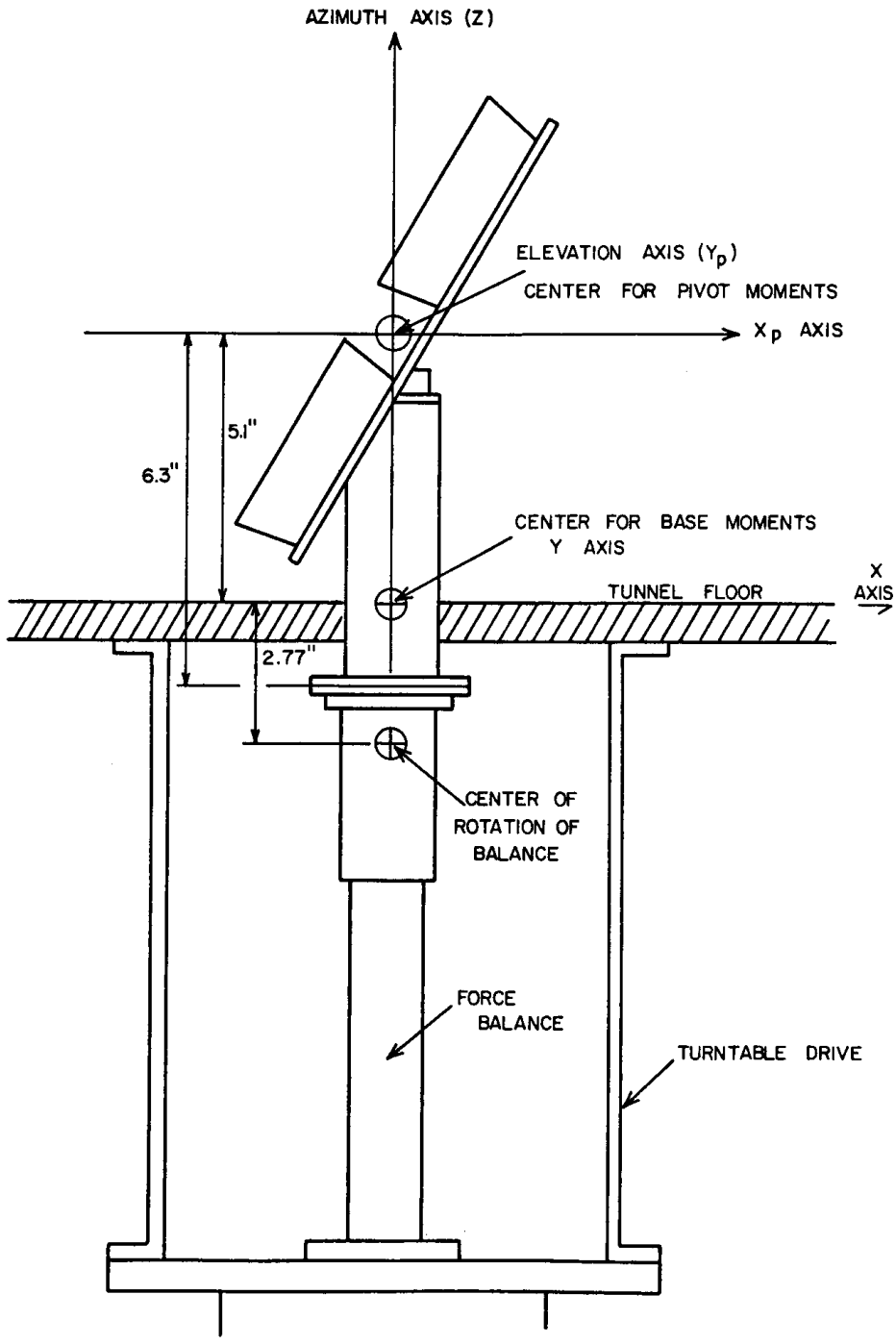


FIGURE 3b. MODEL CONFIGURATION

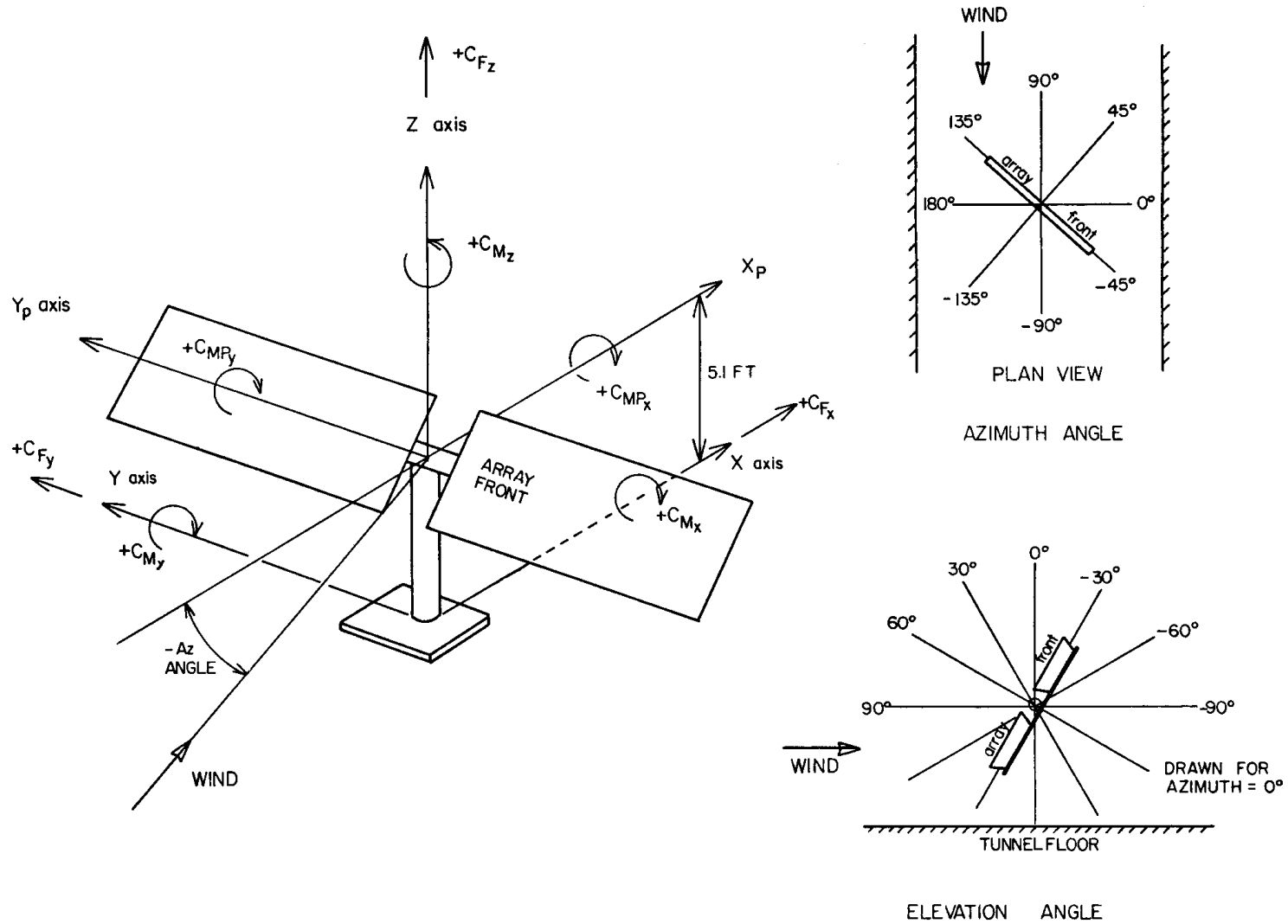


FIGURE 4. DEFINITION OF COORDINATE SYSTEM

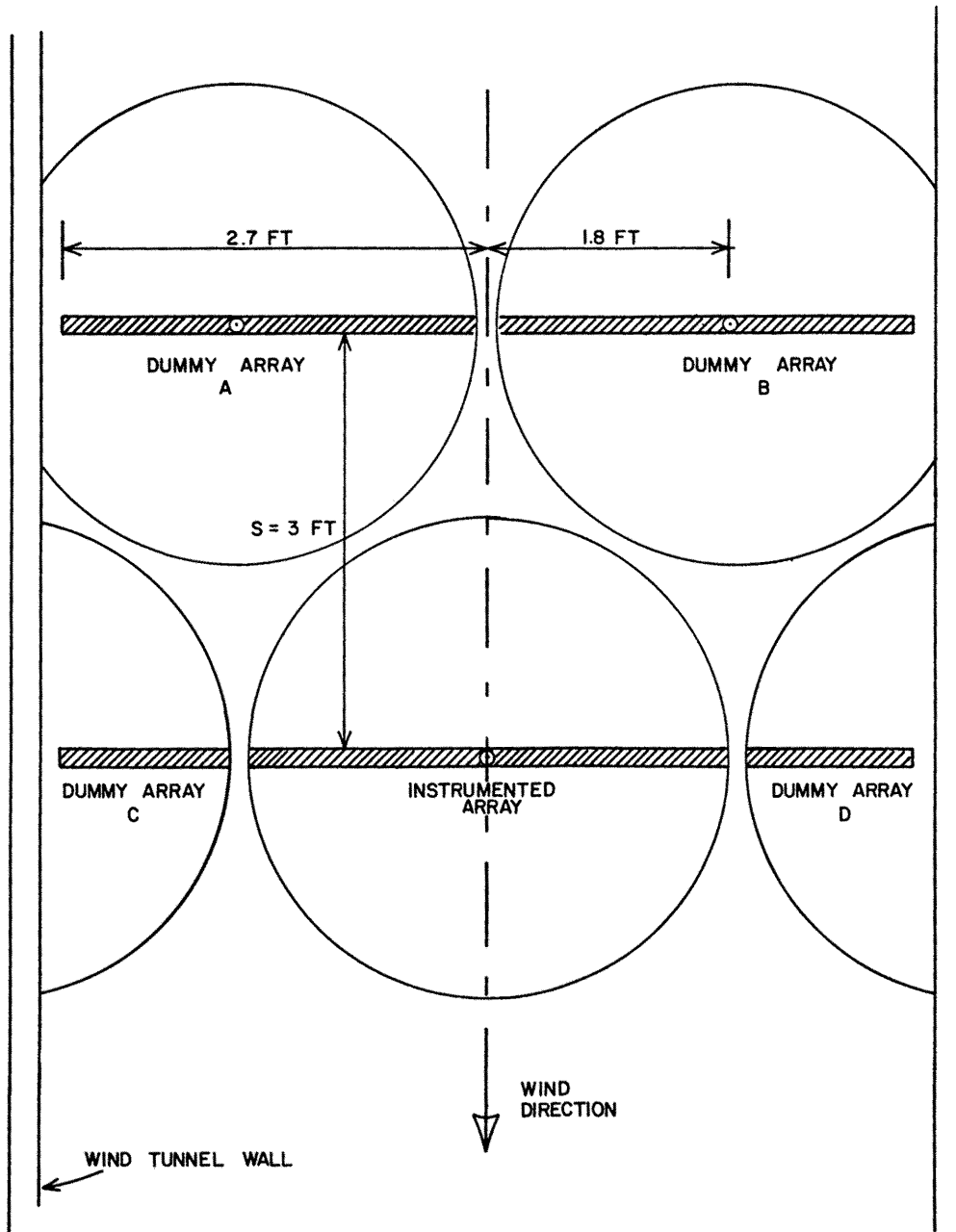


FIGURE 5. ARRAY CLUSTER CONFIGURATION

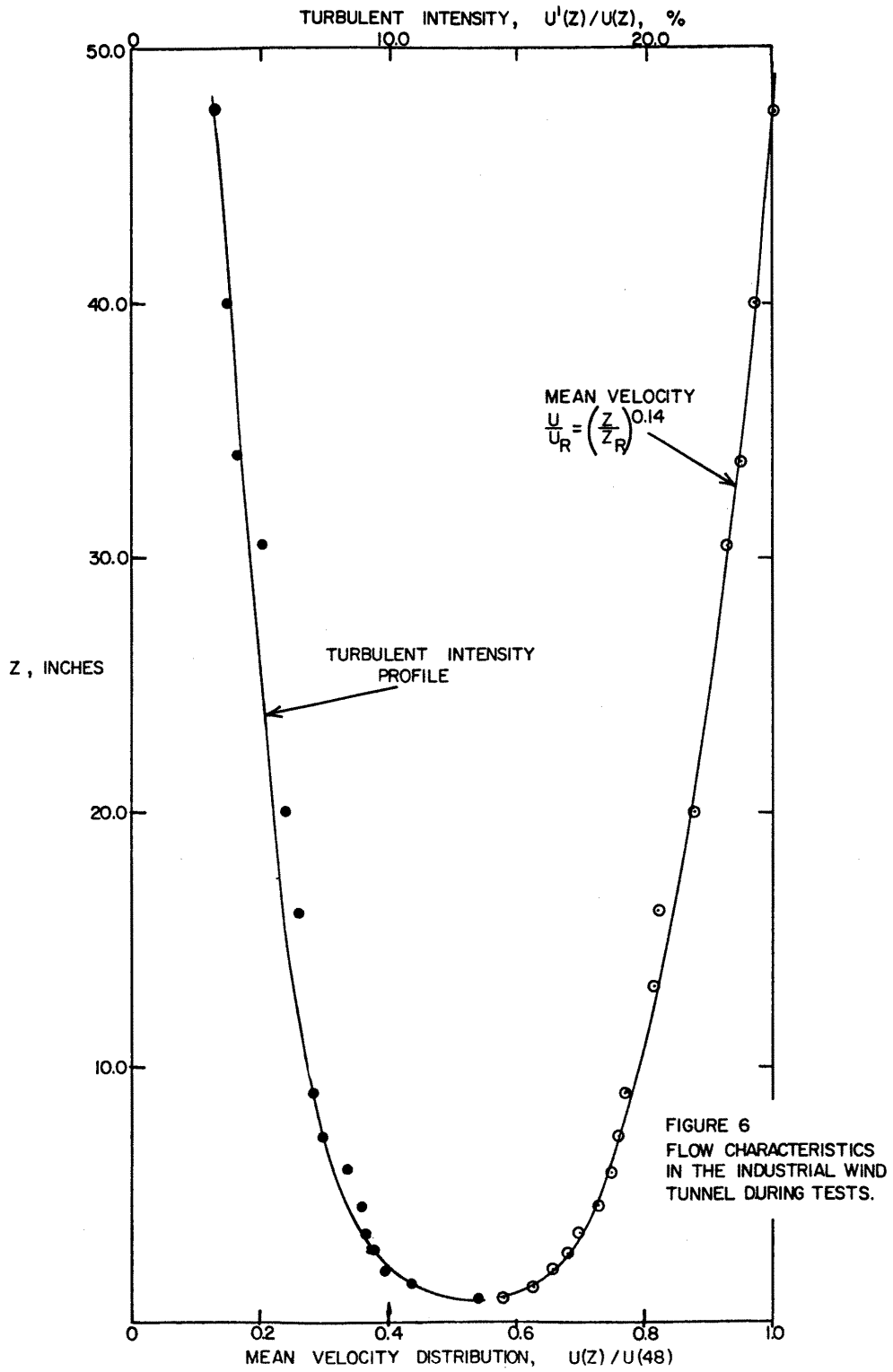


FIGURE 6. FLOW CHARACTERISTICS IN THE INDUSTRIAL WIND TUNNEL DURING TESTS

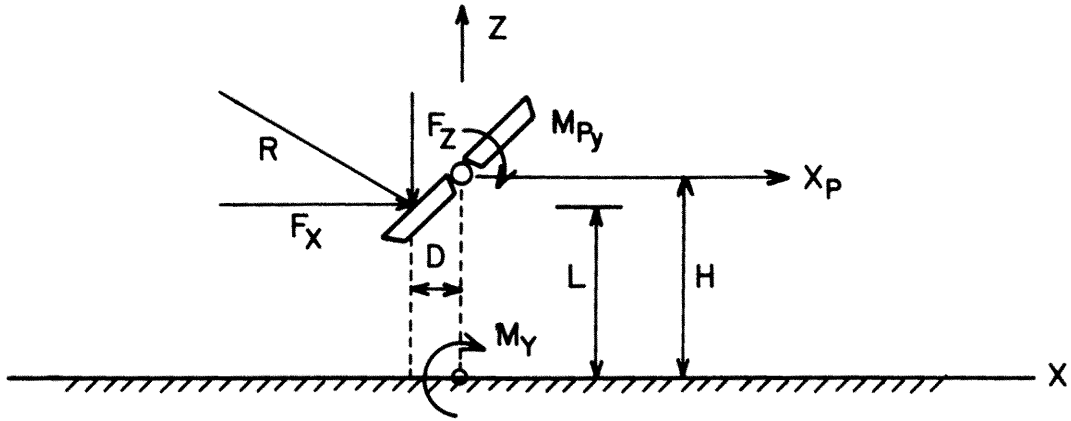


FIGURE 7. MOMENT TRANSFER FROM M_y TO M_{py} .

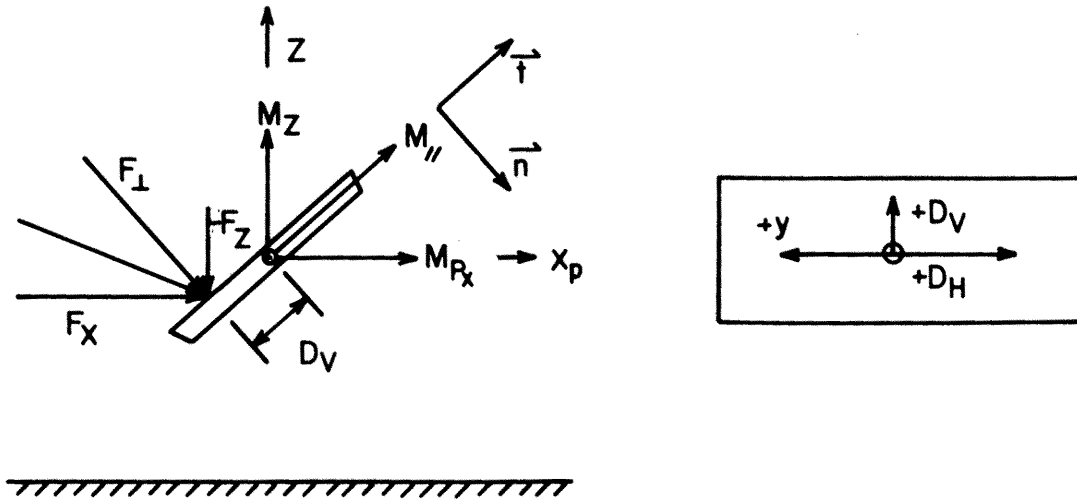


FIGURE 8. DETERMINATION OF CENTER OF PRESSURE

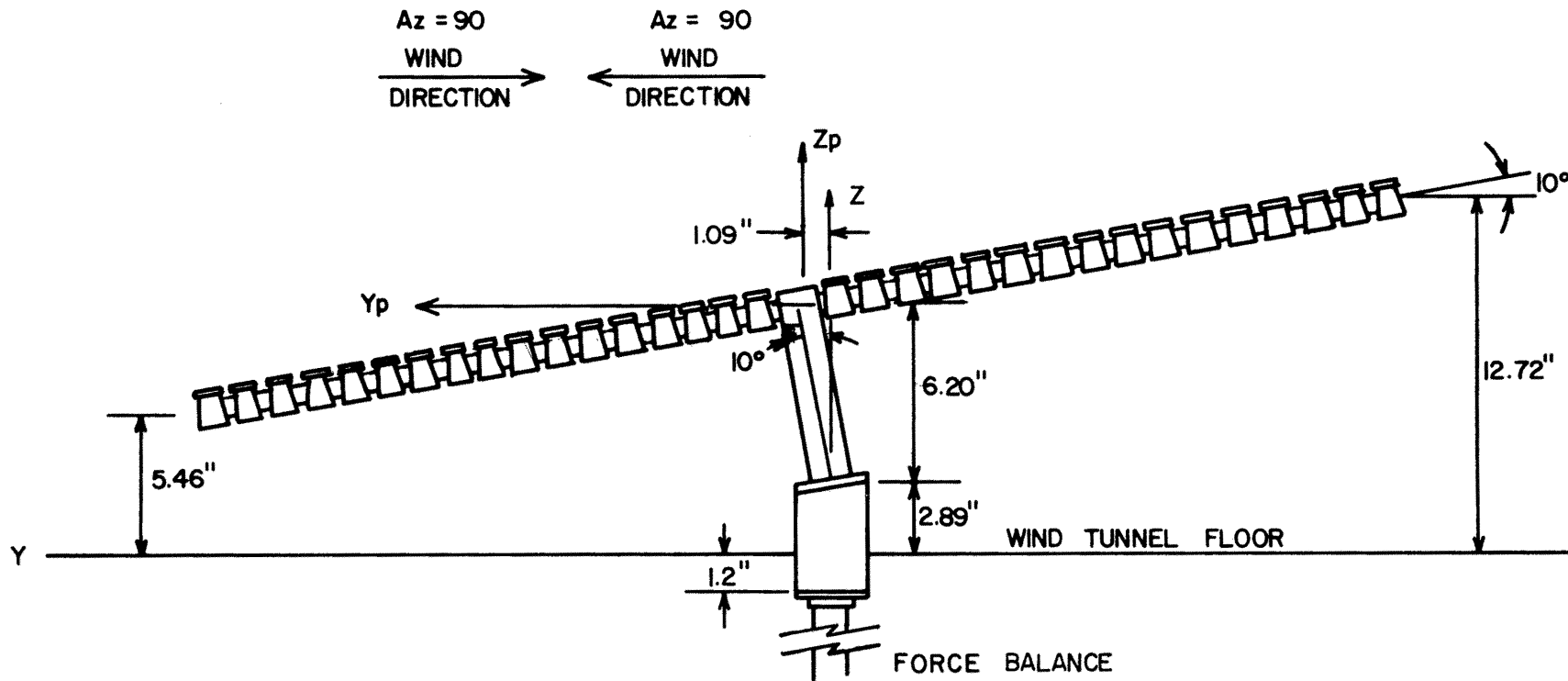
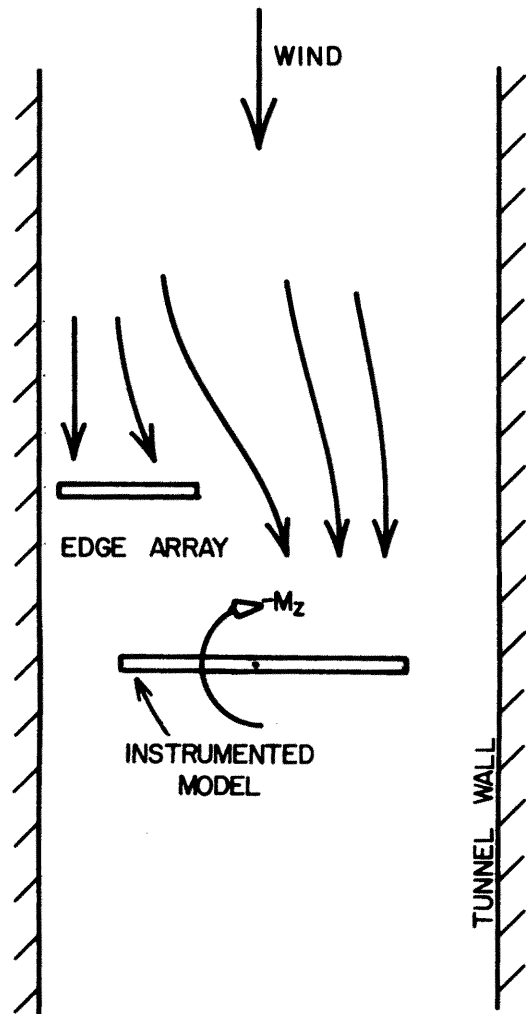
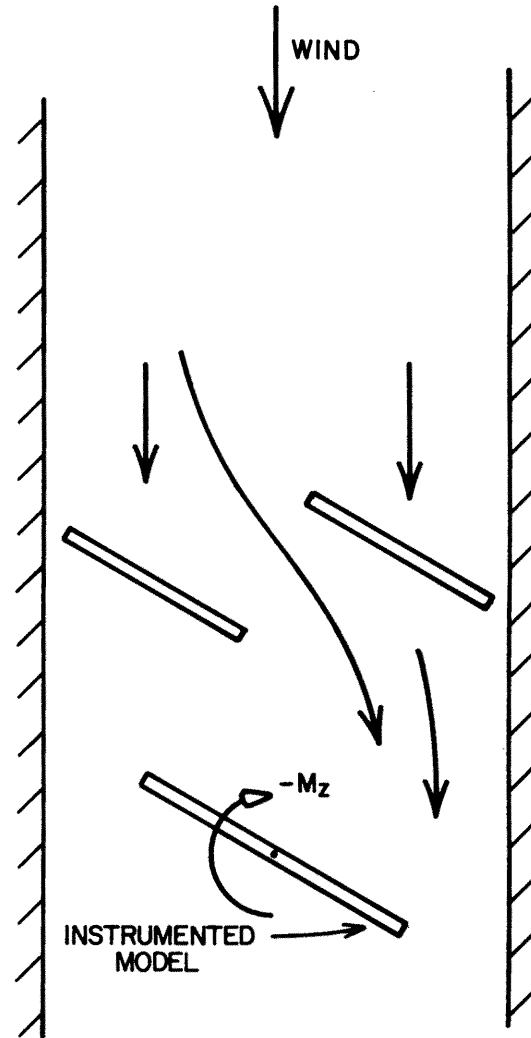


FIGURE 9. ARRAY IN STOWED POSITION AT 10° ANGLE (PART C OF PHASE I)



EL = 0°
 AZ = 0°
 (a)

PLAN VIEW



EL = 0°
 AZ = -30°
 (b)

FIGURE 10 EFFECTS OF ADJACENT ARRAY
 (a) UNBALANCED SHIELDING, (b) CHANNELING